



PREDICTION OF CRACK DEPTH AND POSITION IN VIBRATING BEAMS USING ARTIFICIAL NEURAL NETWORKS

Athanasios BOUBOULAS, Pantelis NIKOLAKOPOULOS, Nikolaos ANIFANTIS

Machine Design Laboratory, Mechanical and Aeronautics Engineering Department, University of Patras, Greece
Corresponding author, e-mail: ampoumpoulas@upatras.gr

Abstract

The aim of this paper is to develop a finite element procedure for crack prediction in vibrating beams. Based on this procedure, full frictional contact conditions are introduced between the crack surfaces in order to consider the breathing of crack. The region surrounding the crack is simulated by two-dimensional finite elements. An incremental-iterative procedure is employed to solve the nonlinear dynamic equations governing this problem. The obtained time response is processed with Fast Fourier Transform to extract its frequency components. The first three natural frequencies are input to a trained Artificial Neural Network for depth and position prediction of the crack. This study is validated for a dynamic loading cantilever beam. It is found that the proposed procedure is capable of predicting the crack depth and position with high accuracy.

Keywords: crack prediction, contact conditions, finite element method, artificial neural networks

1. INTRODUCTION

Beams are used as members in many engineering applications. For various causes, these members often experience cracks under working conditions. The existence of cracks in beams causes variations in stiffness. These variations have influence on the dynamic behavior of the total structure. Thus, the detection of cracks in beams is of utmost importance in structural safety assessment. Direct procedures, based, for example, on acoustic, magnetic field, radiography, have been employed for this purpose. However, most of these procedures are inoperative and unsuitable, since they require time-consuming and expensive inspections [1]. For these reasons, during the past decades, the research interest has turned to alternative procedures in crack detection utilizing vibration parameters [2].

Artificial Neural Networks (ANN) method is a mathematical model inspired by the human brain operation. Due to its ability to approximate continuous functions and to recognize patterns, ANN is used to detect cracks from modal parameters. The basic concept for utilizing ANN in crack detection is the development of a model to relate, via a training process, the modal parameters with structural parameters. When the relation is set up, the trained ANN can identify the cracks position and depth from modal data. In 1992, Wu and co-workers [3] reported for first time the successful application of ANN in crack detection utilizing modal parameters. Since then, many researchers have concluded the potential

of ANN for crack detection in beam-like structures [4-8].

In the aforementioned studies, the cracks are considered continuously open during vibration. In fact, the cracks breathe or in other words open and close regularly causing variations in the beams stiffness which lead the beams to nonlinear dynamic behavior [9]. This behavior generates higher frequency harmonics. In particular, the natural frequencies of beams with a breathing crack are higher than those of beams with an always open crack [10]. Thus, vibration-based methods for crack detection should include breathing crack effects in order to give precise conclusions concerning the state of crack. However, the development of a realistic breathing crack model is a complicated problem [11]. The crack contact state, intermediate between those of fully open and fully closed, can be treated only with a numerical implementation. Ma et al. [12] treated the breathing crack effect as a frictionless contact problem between a rigid and an elastic surface. Long et al. [13] developed a finite element model for a beam with a breathing crack considering that the bending stiffness of beam varies periodically when crack opens and closes during vibration. In authors' previous work [11], a finite element model for a vibrating beam, considering the crack surfaces contact, was presented.

This two-dimensional finite element model in conjunction with Fast Fourier Transform (FFT) and Artificial Neural Networks (ANN) compose a finite element procedure for crack prediction in vibrating

beams. In particular, full frictional contact conditions are involved between the crack surfaces to consider the breathing of crack, while the beam is simulated by two-dimensional finite elements. An incremental-iterative procedure is utilized to solve the nonlinear equations of this dynamic problem. The obtained response is converted from time-domain to frequency-domain employing FFT. The first three natural frequencies are applied as input in a feed-forward multi-layer perceptron ANN. This study is validated for an impulsive loading cantilever beam. It is deduced that the crack characteristics, depth and position, are predicted with a high accuracy compared to the actual ones.

2. FINITE ELEMENT PROCEDURE

2.1. Cracked beam model

In what follows, the Euler-type two-dimensional cantilever beam model of Figure 1 is considered. The beam has length L and cross-section $b \times h$. At a position L_c from its fixed end, the beam contains a non-propagating edge crack of depth a . The surfaces of the crack are considered smooth and the thickness of the crack negligible. A transverse dynamic loading is applied at the tip node A . It is considered that the beam is made of a linear elastic material and undergoes small displacements and strains. The beam is simulated by conventional finite elements as shown in Fig. 2. For reasons of accuracy and compatibility, the two equal length surfaces of the crack are discretized into uniformly spaced three-noded triangular elements. The region surrounding the crack is simulated by three-noded triangular elements. The density of these elements is very high around the crack surfaces and crack tip in order to satisfy the contact conditions when partial crack closure occurs. The remaining beam region is discretized into four-noded quadrilateral elements performing as transition elements.

2.2. Crack surfaces contact

Parts of the crack surfaces $^I S$ and $^{II} S$ may come into contact at an interface $^c S$, defined as $^c S = ^I S \cap ^{II} S$ (Figure 3). The extent of this interface may vary during the interaction of structure and load. It is usually composed of a slipping part and an adhesive part. In this study, the prediction of this interface is based on the master-slave concept. Based on this concept, the $^I S$ is assumed as master surface and the $^{II} S$ as slave surface. These two surfaces are defined in terms of local coordinate systems $(^j x_1, ^j x_2)$, where $j=I$ corresponds to the master surface and $j=II$ to the slave surface. Subscripts 1 and 2 represent the tangential and normal directions, respectively, to the crack surfaces. Both axes $^j x_2$ define the direction of the unit outward normal vector of the corresponding surfaces, while the

corresponding axes $^j x_1$ define the slipping direction. The nodes on the master and slave surfaces are termed, respectively, as master nodes and slave nodes. The contact surface of the master body is covered by contact (master) segments which are defined by two adjacent master nodes. Contact occurs between a node of the slave surface and a point of the master surface that may be located at an edge, a point or a node of the master segment. A master segment can come into contact with not only one slave node at each time. On the contrary, a slave node can come into contact with only one point on the master segment.

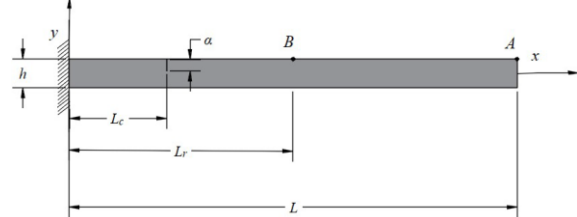


Fig. 1. Cantilever beam model

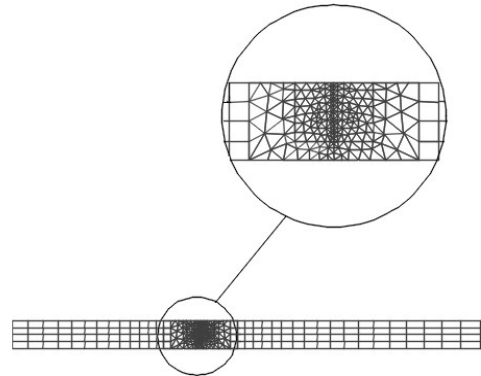


Fig. 2. Typical cracked beam finite element mesh
($a/h = 0.8$ and $L_c/L = 0.5$)

The contact conditions, for each contact pair, are defined in terms of a local coordinate system in the direction of the average normal to the boundaries of the bodies. In what follows, u_i and R_i , with $i=1,2$ represent, respectively, nodal displacement and force components. These components are expressed in respect to the local coordinate systems $(^j x_1, ^j x_2)$, with $j=I, II$ (Fig. 3). For simplicity, the subscripts which represent nodal numbers are omitted. The force components satisfy the following equilibrium equations:

$$^I R_i + ^{II} R_i = 0, \quad i=1, 2. \quad (1)$$

The traction-free conditions for the open crack state are:

$$^I R_i = ^{II} R_i = 0, \quad i=1, 2. \quad (2)$$

For the adhesion state, the displacement components are related by the equations:

$$^I u_1 + ^{II} u_1 = 0. \quad (3)$$

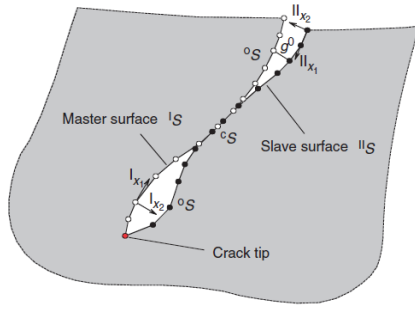


Fig. 3. Crack surfaces contact [11]

In case there is an initial normal gap g^0 between the master and slave nodes of a pair, the displacement components along this direction are:

$$I u_2 + II u_2 = g^0, \quad (4)$$

For the slip state, the tangential and normal force components are related by the equations:

$$I R_1 \pm \mu I R_2 = 0, \quad (5)$$

where μ the coefficient of Coulomb friction. Furthermore, the equation (4) is valid, since the slip allows the occurrence of a gap between the crack surfaces.

2.3. Incremental-iterative procedure

The nonlinear dynamic behavior of the beam model is described by the equations:

$$\mathbf{M}\ddot{\mathbf{U}} + \mathbf{C}\dot{\mathbf{U}} + \mathbf{K}\mathbf{U} = \mathbf{R}. \quad (6)$$

In the above equations, \mathbf{M} is the mass matrix, \mathbf{C} is the damping matrix and \mathbf{K} is the stiffness matrix. The superimposed dot represents derivative with respect to time. Thus, $\ddot{\mathbf{U}}$ is the nodal accelerations vector, $\dot{\mathbf{U}}$ is the nodal velocities vector, \mathbf{U} is the nodal displacements vector and \mathbf{R} is the external forces vector. These vectors are defined in respect of a global Cartesian coordinate system x, y, z .

An implicit direct integration scheme is utilized to solve the nonlinear equations (6). According to this scheme, the solution time interval of interest $[0, T]$ is subdivided into N equal time increments Δt , where $\Delta t = T/N$. Approximate solutions of equations (6) are sought at times $0, \Delta t, 2\Delta t, \dots, t, t + \Delta t, \dots, T$. The solution at a specific time requires that the solutions of all previous times are known. Based on the modified Newton-Raphson method, for time $t + \Delta t$ and iteration k the equations (6) are written as [14]:

$${}^t \mathbf{K}_T \Delta \mathbf{U}^{(k)} = \Delta \mathbf{R}^{(k-1)}, \quad (7)$$

$${}^{t+\Delta t} \mathbf{U}^{(k)} = {}^{t+\Delta t} \mathbf{U}^{(k-1)} + \Delta \mathbf{U}^{(k)}. \quad (8)$$

In the above two equations, ${}^t \mathbf{K}_T$ is a linear combination of the mass matrix, damping matrix and tangential stiffness matrix. $\Delta \mathbf{U}^{(k)}$ is the incremental nodal displacement vector and $\Delta \mathbf{R}^{(k-1)}$ is a function of the nodal force vector and contributions from the damping and inertia of the system. In each iteration,

the incremental displacement vector $\Delta \mathbf{U}^{(k)}$ is derived by solution of equations (7), since the vector $\Delta \mathbf{R}^{(k-1)}$ is known from the most recent displacements and the matrix ${}^t \mathbf{K}_T$ is also known for the calculations of the time t . The vector ${}^{t+\Delta t} \mathbf{U}^{(k)}$ is obtained from equations (8). To calculate displacement and force vectors for time $t + \Delta t$, the equations (1)-(5) are written in incremental form [11]. Then, they are transformed in respect to a global coordinate system x, y, z and assembled in equations (7) and (8). Initially, the employed iterative procedure considers the convergent contact status of the previous time t . Furthermore, it considers that the incremental force components for master surface at time $t + \Delta t$ are zero. The contact state for each node pair is examined and appropriate changes are implemented to identify the equilibrium state of the contact conditions [11]. The incremental vectors ${}^{t+\Delta t} \Delta \mathbf{U}$ and ${}^{t+\Delta t} \Delta \mathbf{R}$ are known for the total structure, when the iterative procedure converges. Then, the procedure goes to the next time increment and continues until the final one is reached. The obtained time response is processed with FFT to extract its frequency components [15].

2.4. Artificial neural networks

According to John McCarthy, Artificial Intelligence (AI) is "the science and engineering of making intelligent machines" [16]. ANN is a type of AI that is inspired by the structure and function of the human brain. Key properties of ANN are the capability of pattern recognition and classification, data interpretation and function approximation. ANN provides a nonlinear parameterised mapping between input and output data. The networks are arranged in layers of input, hidden and output neurons, which are massively interconnected. The layers are linked by transfer functions and the neurons weighted by adjustable variables. There are many different ANN types with different topologies. The most widely used networks in crack detection are feed-forward multi-layer perceptron (MLP).

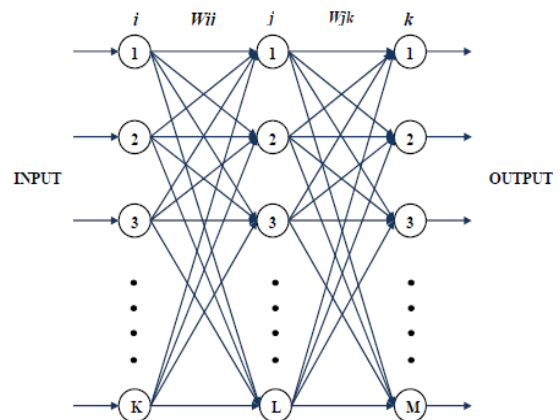


Fig. 4. Schematic diagram of a three-layered MLP network

Figure 4 shows a MLP network with layers i , j and k and interconnection weights W_{ij} and W_{jk} between the layers of the neurons. In the training process, the initial assigned weights are continuously corrected. In particular, the predicted outputs (obtained from MLP) are compared with the real ones and the errors are back propagated (from right to left in Figure 4). Based on this algorithm, the weights are corrected or adjusted and the errors are minimized. In the present study, the adjusting of weights is performed with Levenberg-Marquardt algorithm [17, 18].

3. NUMERICAL RESULTS

The present method is assessed for the beam model of Figure 1. It is considered that the beam has a length of $L=1.5$ m and a cross-section of $b \times h = 0.075 \text{ m} \times 0.075 \text{ m} = 5.625 \times 10^{-3} \text{ m}^2$. The adopted beam material is carbon steel with modulus of elasticity $E = 2.06 \times 10^{11} \text{ Pa}$, mass density $\rho = 7650 \text{ kg/m}^3$ and Poisson's ratio $\nu = 0.29$. Four different dimensionless crack positions are considered, $L_c/L = 0.2, 0.4, 0.6, 0.8$. For each one of these positions, the dimensionless crack depths $a/h = 0.2, 0.4, 0.6, 0.8$ are investigated. Lower depths ($a/h < 0.2$) are not considered, since small cracks have a slight influence on the vibration-based crack detection methods [19]. The beam undergoes a transverse impulse loading of 100 N at point A, from time $t=0$ to time $t=\Delta t$ (Figure 1). The transverse acceleration response is acquired from node B which is at a dimensionless position $L_r/L=1$ from the fixed end (at position of point A). For all considered cracked beams, the corresponding finite element meshes consist of approximately the same number of each type of elements and nodes. For instance, the mesh of a beam with a crack of $a/h=0.8$ and $L_c/L=0.5$ is composed of 1002 three-noded triangular 201 four-noded quadrilateral elements and 797 nodes. Numerical experimentations demonstrate that higher densities of elements in the vicinity of the crack have slight influence on the results (less than 1%). For the beam without the crack, the finite element mesh consists of 160 uniform four-noded quadrilateral elements and 205 nodes. The damping loss factor ($C=0$) is ignored, since it is very small for all the carbon steel beams considered in this study. This factor affects mainly the magnitude of the modal analysis, performed below. The natural frequencies are nearly unaffected. Initially, (at time $t=0$), the nodal displacements, velocities and accelerations vectors are assumed as ${}^0\mathbf{U}=0$, ${}^0\dot{\mathbf{U}}=0$, ${}^0\ddot{\mathbf{U}}=0$. The Newmark method, which is commonly used in time

integration schemes, is employed with $\delta=1/2$ and $\alpha=1/4$. The time increment is considered as $\Delta t=1 \times 10^{-5}$ sec. Convergence studies show that smaller time increments have a slight influence on the results (less than 1%). A sensitivity analysis demonstrates that, for the considered smooth crack surfaces, the results are influenced less than 0.5% by the coefficient of friction. Thus, the results presented below for $\mu=0.1$ should be reasonably unaffected for most of the considered crack cases. Equations (8) are solved again and again until the convergence criterions satisfied [11]. For all considered cracked beams, the maximum three iterations are required between two subsequent sequences. This happens due to the small crack surfaces and the dense finite element mesh in vicinity of the crack. The impulsive transverse acceleration response at node B is analyzed with FFT in order to extract its frequency components. For reasons of comparisons, the linear dynamic problems of the beam without and an always open crack are considered. These two problems are solved using the above finite element procedure ignoring equations (1)-(5).

To show the accuracy of the present study, the first three natural frequencies of beams without crack and with an open or a breathing crack of $L_c/L=0.5$ and $a/h=0.5$ are extracted from the FFTs of corresponding impulsive responses. For the first two cases comparisons are performed with the results obtained from an eigenvalue finite element procedure [14], while for the third case with the results reported in the work of Nandwana and Maiti [20]. The maximum percentage difference, for all considered cases does not exceed 1.61%.

Figure 5 shows the FFTs of the impulsive responses for a beam with either an open or a breathing crack of $a/h=0.2$ and $L_c/L=0.2$. The three vertical lines correspond to the loci of the first

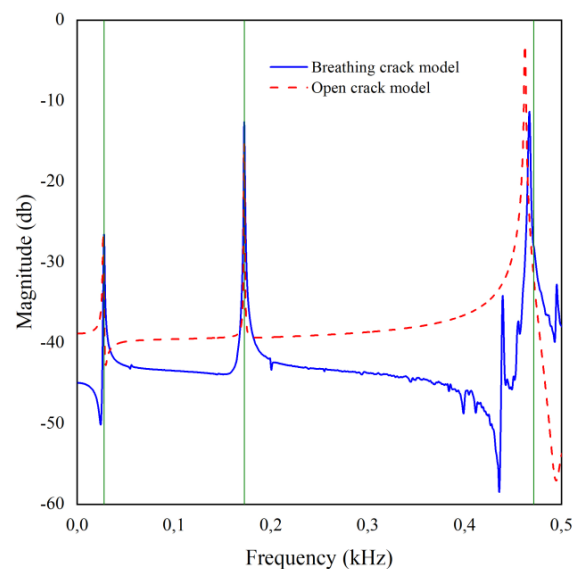


Fig. 5. FFT of impulsive response for a crack of $a/h=0.2$ and $L_c/L=0.2$

three natural bending frequencies of the noncracked beam, obtained from FFT of the corresponding impulsive response. It is observed that the first two natural frequencies of these two crack models are close and are lower than those of the intact beam. The third frequency of the breathing crack model is between those of the open cracked model and the intact beam, as expected [10]. The identification of the primary peaks for the breathing model requires further investigation, which is out of the scope of this work. They are caused by crack contact and vibrations of the fractured beam and beam portions aside the crack.

For all considered crack cases, the first three dimensionless natural frequencies f_{ic}/f_{iu} of the faulty beams are extracted from FFTs of the corresponding impulsive responses. The subscript $i=1,2,3$ denotes the order of the natural frequency and subscripts u, c the noncracked and cracked state of the beam, respectively. The natural frequencies are

the inputs to the ANN and the crack depth and position the outputs. Many ANN models were tested. In each model, a different number of hidden layers with various numbers of neurons were used. The effect of transfer functions was also investigated. Apart from the input and output layers, the designed ANN has two hidden layers. The first of these two hidden layers contains 30 neurons and the second 15 neurons. The tangent sigmoid transfer function is applied to all layers. The ANN model was designed and implemented using the Matlab neural network toolbox with Levenberg–Marquardt algorithm. The regression analysis of training, validation and test data is shown in Figure 6 which shows that predicted data are well fitted to the actual ones. In particular, the absolute percentage difference between these two set lies between 0% and 4.9% (Table 1).

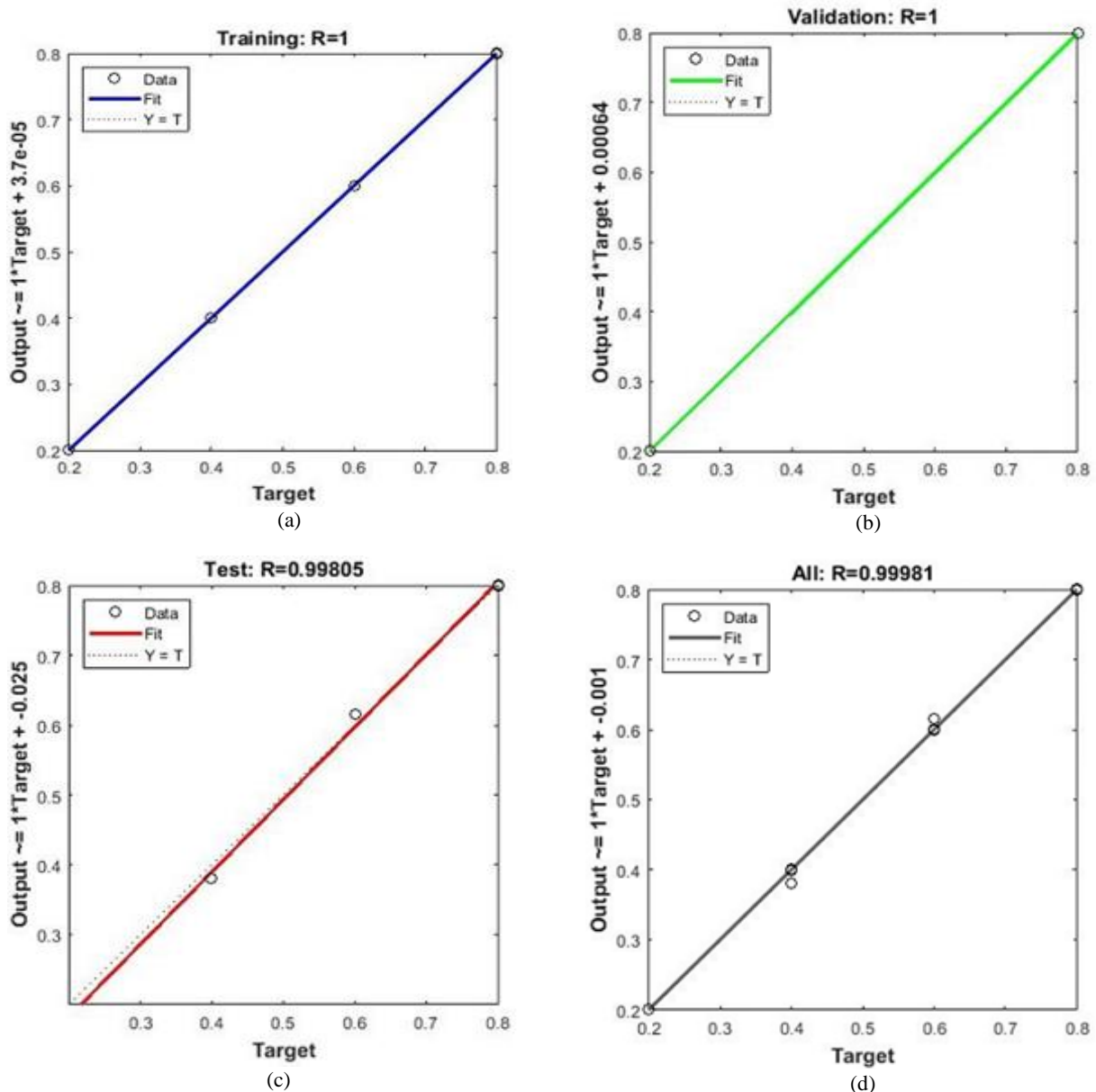


Fig. 6. Regression plot of: (a) training, (b) validation, (c) testing and (d) general set

Table 1. Comparisons between actual and predicted crack characteristics

Actual		Predicted		Percentage differences	
a/h	L_c/L	a/h	L_c/L	a/h	L_c/L
0.2	0.2	0.2000	0.2006	0	0.3
0.2	0.4	0.3999	0.2000	0	0
0.2	0.6	0.6000	0.2000	0	0
0.2	0.8	0.7989	0.2000	-0.1	0
0.4	0.2	0.2000	0.4000	0	0
0.4	0.4	0.3999	0.4000	0	0
0.4	0.6	0.6000	0.4000	0	0
0.4	0.8	0.7999	0.3804	0	-4.9
0.6	0.2	0.2000	0.6000	0	0
0.6	0.4	0.3999	0.6000	0	0
0.6	0.6	0.6000	0.6000	0	0
0.6	0.8	0.7999	0.6000	0	0
0.8	0.2	0.2000	0.7999	0	0
0.8	0.4	0.4000	0.8000	0	0
0.8	0.6	0.6150	0.8000	2.6	0
0.8	0.8	0.7999	0.8000	0	0

4. CONCLUSIONS

A finite element procedure for crack prediction in vibrating beams is formulated in this paper. Based on this procedure, full frictional contact conditions are involved between the crack surfaces to consider the breathing of crack, while the beam is simulated by two-dimensional finite elements. An incremental-iterative procedure is employed to treat the nonlinear dynamic equations for this model. The extracted response is converted from time-domain to frequency-domain using Fast Fourier Transform. The first three natural frequencies are applied as input in a feed-forward multi-layer perceptron Artificial Neural Network for prediction of crack characteristics. The present study is validated for a cracked cantilever beam under an impulse loading. It is deduced that the crack depth and position are predicted with a high accuracy (around 5%) compared to the actual ones.

Author contributions: *research concept and design, P.N., N.A.; Collection and/or assembly of data, A.B.; Data analysis and interpretation, A.B.; Writing the article, A.B.; Critical revision of the article, P.N.; Final approval of the article, A.B., P.N., N.A.*

Declaration of competing interest: *The authors declare that they have no known competing financial interests or personal relationships that could have appeared to influence the work reported in this paper.*

REFERENCES

- Montalvão E, Silva JM, Araújo Gomes AJM. Experimental dynamic analysis of cracked free-free beams. *Experimental Mechanics* 1990; 30:20–25. <https://doi.org/10.1007/BF02322697>.
- Doebbling SW, Farrar CR, Prime MB. A summary review of vibration-based damage identification methods. *Shock and Vibration Digest* 1998; 30 (2):91–105.
- Wu X, Ghaboussi J, Garrett JH. Use of neural networks in detection of structural damage. *Computers & Structures* 1992;42(4):649–659. [https://doi.org/10.1016/0045-7949\(92\)90132-J](https://doi.org/10.1016/0045-7949(92)90132-J).
- Nazari F, Abolbashari MH. Double cracks identification in functionally graded beams using artificial neural network. *Journal of Solid Mechanics* 2013; 5(1):14–21.
- Aydin K, Kisi O. Damage diagnosis in beam-like structures by artificial neural networks. *Journal of Civil Engineering and Management* 2015; 21(5):591–604. <https://doi.org/10.3846/13923730.2014.890663>.
- Gowd BP, Jayasree K., Hegde MN. Comparison of artificial neural networks and fuzzy logic approaches for crack detection in a beam like structure. *International Journal of Artificial Intelligence and Applications* 2018;9(1):35–52. <https://doi.org/10.5121/ijaiia.2018.9103>.
- Kekan AH, Kumar BR. Crack depth and crack location identification using artificial neural network. *International Journal of Mechanical Production Engineering Research and Development* 2019; 9(2): 699–708.
- Maurya M, Sadarang J, Panigrahi I. Detection of crack in structure using dynamic analysis and artificial neural network. *Engineering Solid Mechanics* 2020; 8(3): 285–300. <https://doi.org/10.5267/j.esm.2019.11.002>.
- Gudmunson P. The dynamic behavior of slender structures with cross-sectional cracks. *Journal of the Mechanics and Physics of Solids* 1983; 31(4):329–345. [https://doi.org/10.1016/0022-5096\(83\)90003-0](https://doi.org/10.1016/0022-5096(83)90003-0).
- Shen MH, Chu YC. Vibrations of beams with a fatigue crack. *Computers and Structures* 1992; 45(1):79–93. [https://doi.org/10.1016/0045-7949\(92\)90347-3](https://doi.org/10.1016/0045-7949(92)90347-3).
- Bouboulas AS, Anifantis NK. Finite element modeling of a vibrating beam with a breathing crack: observations on crack detection. *Structural Health Monitoring* 2011; 10(2):131–145. <https://doi.org/10.1177%2F1475921710373286>.
- Ma H, Zeng J, Lang Z, Zhang L, Guo Y, Wen B. Analysis of the dynamic characteristics of a slant-cracked cantilever beam. *Mechanical Systems and Signal Processing* 2016; 75, 261–279. <https://doi.org/10.1016/j.ymssp.2015.12.009>.
- Long H, Liu Y, Liu K. Nonlinear Vibration Analysis of a Beam with a Breathing Crack. *Applied Sciences* 2019;9(18):3874. <https://doi.org/10.3390/app9183874>.

14. Bathe, K.J. Finite Element Procedures. Prentice-Hall, Upper Saddle River, NJ, 1996.
15. Brigham EO. The Fast Fourier and Applications. Englewood Cliffs, NJ: Prentice Hall, 1988.
16. McCarthy J. Ascribing mental qualities to machines. In Martin Ringle (ed.), Philosophical Perspectives in Artificial Intelligence, Humanities Press, 1979.
17. Marquardt DW. An algorithm for least squares estimation of non-linear parameters. Journal of the Society for Industrial and Applied Mathematics 1963; 11(2):431–441. <https://doi.org/10.1137/0111030>.
18. Hagan MT, Menhaj MB. Training feed forward networks with the Marquardt algorithm. IEEE Transactions on Neural Networks 1994; 5(6):889–993. <https://doi.org/10.1109/72.329697>.
19. Dimarogonas AD. Vibration of cracked structures: A state of the art review. Engineering Fracture Mechanics 1996; 55(5):831-857. [https://doi.org/10.1016/0013-7944\(94\)00175-8](https://doi.org/10.1016/0013-7944(94)00175-8).
20. Nandwana BP, Maiti SK. Modelling of vibration of beam in presence of inclined edge or internal crack for its possible detection based on frequency measurements. Engineering Fracture Mechanics 1997; 58(3):193-205. [https://doi.org/10.1016/S0013-7944\(97\)00078-7](https://doi.org/10.1016/S0013-7944(97)00078-7).



Athanasios BOUBOULAS, Doctor in the Faculty of Mechanical Engineering and Aeronautics at University of Patras. His current research interests include structural design and analysis employing Finite element method.



Pantelis NIKOLAKOPOULOS, Associate Professor in the Mechanical Engineering & Aeronautics at University of Patras. His current research interests include, Design via simulations, experiments in Tribology of Machine Elements and fault detection



Nikolaos ANYFANTIS, Professor, in the Mechanical Engineering & Aeronautics at University of Patras. His current research interests include, Design of Machine Elements and nanomechanics via simulations

Received 2022-07-17
Accepted 2022-09-19
Available online 2022-09-20